USING STRUCTURE FROM MOTION AND HIGH-RESOLUTION DIGITAL ELEVATION MODELS TO INVESTIGATE THE RELATIONSHIPS BETWEEN EMPLACEMENT HISTORY AND LAVA SURFACE ROUGHNESS: MAUNA ULU (HI), AMBOY (CA), AND THARSIS. D. H. James[1] and S.W. Anderson[1], [1]University of Northern Colorado (Campus Box 100, 501 20th St, Greeley, CO 80639, Davitia.James@unco.edu, steven.anderson@unco.edu).

Introduction: Roughness patterns reveal lava flow surface features when observed at different scales [1-3]. These features can be tied to emplacement conditions using recorded observations of active basaltic volcanoes. Patterns of roughness across a lava flow are therefore related to eruption characteristics such as rate of flow, viscosity, and underlying slope [1,4,5]. This project aims to use structure from motion software to create high-resolution (cm to sub cm-scale) digital elevation models (DEMs) of terrestrial lava flows, along with High Resolution Imaging Science Experiment (HiRISE) and Context camera (CTX) derived DEMs, to develop a method for interpreting morphological features on extraterrestrial lava flows using surface roughness measurements. This will further our understanding of emplacement rates and styles during the volcanically active period of Mars' history and may also provide insight regarding terrestrial volcanism [3,6,7,8].

Dust deposition affects roughness across the majority of the martian surface. Small lava flow surface features such as cracks and folds are the first to be hidden as a result of mantling. It is unclear if larger, underlying lava flow features can be identified based on remaining roughness elements after significant mantling. Hesperian plains on Mars are buried up to several meters in many areas, limiting visibility of volcanic features (9,10).

Geologic Settings: All three of our focus areas are characterized by mafic volcanism. Differences in flow morphology are a result of emplacement conditions such as underlying topography, cooling rate, emplacement rate, and extrusion style [1,11]. These sites vary in their degree of mantling by aeolian deposits.

Mauna Ulu, Hawaii. Mauna Ulu, a small shield volcano along Kilauea's East Rift Zone, was last active from 1969-1974. During this period it displayed a variety of eruption styles and produced an extensive (~62 km^2) flow field [12,13]. If relationships exist between remotely sensed roughness variables and emplacement characteristics at Mauna Ulu, they may provide insight into eruptive processes occurring in other, more remote or less studied locations. The flows here are essentially unweathered and unmantled at the scale of our study.

Amboy, California. Amboy Crater is an extinct, ~79 ka cinder cone in the eastern Mojave desert [14]. The Amboy lava field surrounds the crater and covers an approximately 70 km^2 area [15,3]. The adjacent mountains provide a steady supply of sand-sized sediment and wind direction is predominantly south-east based on the wind streaks (Fig. 2). Lava flows at Amboy are moderately to heavily mantled, and are affected by aeolian and, to a lesser extent, fluvial processes [16, 17].

Tharsis, Mars. Massive volcanism during the Hesperian epoch produced widespread basaltic lava flows [18]. Small-scale lava features are a key element to fully understanding eruption conditions. To this end, [19] described the connection between features such as pressure ridges and tumuli to volcanic history of Mars.

We are using structure from motion software (Agisoft) to create high-resolution DEMs of terrestrial basaltic lava flows, along with available Digital Terrain Models (DTMs) of Tharsis flows, to describe the roughness of these flows, as well as the resolutions at which features are visible. We will also quantify any effects of wind-blown mantling on roughness.

Methodology: Medium-scale martian lava flow surface features (~1m on the ground) are resolvable using topographic data from the HiRISE and CTX cameras aboard the Mars Reconnaissance Orbiter. HiRISE DTMs have been used to describe roughness on a submeter scale in the Athabasca region of Mars [20]. Mauna Ulu and Amboy Crater were used as terrestrial analogues because of the range of lava flow surface features visible on these flows, and their similarities to flow surfaces found in Tharsis.

Mauna Ulu offers an opportunity to observe young flows, but the dominant weathering processes in this humid, tropical location are significantly different from processes active on Mars [12]. We selected a 50-meter by 50-meter area on the 1969-74 pahoehoe.

Figure 1. *3D model of a section of the Mauna Ulu site. This area depicted in the image is 0.5m across.*

Using a Nikon D3300 digital single-lens reflex (DSLR) camera and fixed focal length of 24 mm, we photographed the surface of this flow, maintaining at least 60% overlap between all frames to reduce gaps in

the 3D recreation of the site. The Mauna Ulu 3D model (Fig. 1) compiles over 3000 photos.

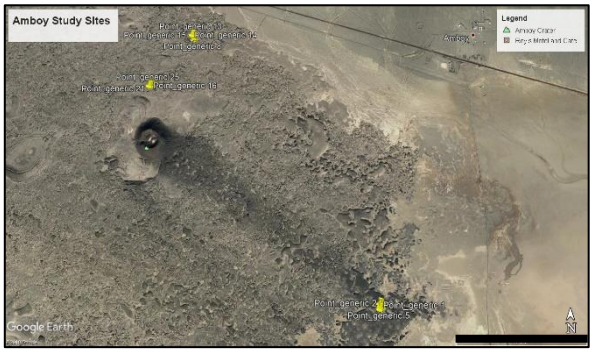

Figure 2. *Satellite image showing Amboy sites and wind streaks. Scale bar is 1 km.*

Lava flows at Amboy are older than those at Mauna Ulu, and display varying levels of mantling by wind-blown sand. At Amboy, the method of field work was the same, except instead of a single, large study area we chose four smaller sites around the crater and, and on and off the wind streak (Fig. 2) to ensure a variety of topographic features, scales and sand quantities were represented. Mauna Ulu's pristine flows provide roughness values of fresh lava surfaces (Fig. 3), whereas Amboy's older lava flows vary from nearly pristine to heavily mantled.

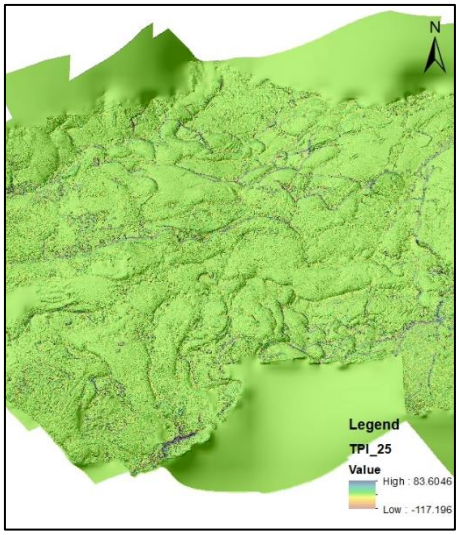

Figure 3. A *Roughness map of a section of the Mauna Ulu site. Cell neighborhood is 25. The area depicted in the image is 5m across.*

Using data from both locations, we will determine how roughness of lava fields containing small-scale features are affected by varying degrees of mantling, where martian lava flows fit into the range of roughness observations at both terrestrial analogue sites, and if these data can be used interpret Mars emplacement conditions. Data from photo surveys of both analogue sites at a range of resolutions to determine which scale is the most effective for identifying and describing volcanic features based on roughness. This will confirm the resolution necessary to classify similar features on Mars [21,22]. This project will utilize the Jenness Topographic Position Index (TPI) extension for ArcGIS to calculate roughness values across the DEM, and create groupings of similar values within the study area. The TPI extension uses detrended elevation grid data to automatically categorize each cell based on the elevation and slope of neighboring cells. A positive result indicates that the cell is higher in elevation (or more steeply sloping) than its neighbors, whereas a negative value shows the cell is lower. Each cell is classified by the magnitude of the difference in elevation along with the slope value. The cell neighborhood can be adjusted to produce varying TPI values for different scales, which changes the scale of roughness being measured (Fig. 3) [23].

The technique presented here may allow us to discern finer features in flow fields than previously possible, thus providing new insights about the quantitative relationships between surface morphology and eruption characteristics.

References: [1] Byrnes J.M. and Crown D. A. (2002) *JGR, 107*, 5079. [2] Mallonee H.C. et al. (2017) *LPSC XLVIII* abstract #2975. [3] Finnegan D. C. et al. (2004) *LPSC XXXV* abstract #1736. [4] Fink J. H. and Anderson S. W. (2000) *in Encyclopedia of Volcanoes, 1*, 307-320. [5] Mallonee H. C. et al. (2017) *LPS XLVIII*, abstract #2992. [6] Fan K.A. et al. (2018) *LPSC LXIX* abstract #2526. [7] Tolometti G. D. et al. (2017) *LPSC XLVIII* abstract #1643. [8] Zanetti M. et al. (2018) *LPSC LXIX* abstract #2361. [9] Rogers A. D. and Head J. W. (2017) *LPSC XLVIII* abstract #1347. [10] Tanaka K. L. (2000), *Icarus, 144*, 254-266. [11] Guest, J. E., et al. (1987) Bull. Volc., 49, 527 – 540. [12] Byrnes J. M. et al. (2004) *JGR, 135*, 169-193. [13] Moncrief S. R. and Rowland S. K., (1991) *LPSC XXII*, 913-914. [14] Philips F. M. (2003) *Geomorphology, 53*, 199-208. [15] Chesterman et al. 1971. [16] Byrnes et al. (2007) *LPSC XXXVIII* abstract #1908. [17] Kienenberger R. L. and Greeley R. (2011) *42nd LPSC*, abstract #1053. [18] Kreslavsky and Head (2000) *JGR, 105*, 695-711. [19] Theilig E. and Greeley R. (1986) *JGR, 91*, 193-206. [20] Kim J. R. and Muller J. P (2008) *Intl. Archives of Photogrammetry, Rem. Sensing and Spatial Info. Sci. XXXVII* 993-998. [21] Whelley P. L. et al. (2014) *Transactions on Geoscience and Remote Sensing, 52*, 426-438. [22] Simurda C.M. (2018) *LPSC LXIX*, abstract #2612. [23] Jenness, J. (2006), TPI extension for ArcGIS, (http://www.jennessent.com/arcview/tpi.htm).